Materials Science in Semiconductor Processing 157 (2023) 107328

Contents lists available at ScienceDirect

Materials Science in Semiconductor Processing

journal homepage: www.elsevier.com/locate/mssp

Laser crystallization of amorphous TiO_2 on polymer

Massimo Zimbone [a], Maria Cantarella [a,*], Federico Giuffrida [a,b], Francesco La Via [c], Vittorio Privitera [c], Enrico Napolitani [a,d], Giuliana Impellizzeri [a]

[a] CNR-IMM, Via S. Sofia 64, 95123, Catania, Italy
[b] Department of Physics and Astronomy, University of Catania, Via Santa Sofia 64, 95123, Catania, Italy
[c] CNR-IMM, Z.I. VIII Strada 5, 95121, Catania, Italy
[d] Department of Physics and Astronomy, University of Padova, Via Marzolo 8, 35131, Padova, Italy

ARTICLE INFO

Keywords:
TiO2
Polymer
Polymethyl methacrylate
Atomic layer deposition
Pulsed UV-laser
Crystallization

ABSTRACT

The deposition of crystalline TiO_2 on polymers can boost its use in a large plethora of applications. In this work, we deposited, through the low-temperature atomic layer deposition (LT-ALD) technique, a thin layer of amorphous TiO_2 on polymethyl-methacrylate (PMMA), and afterwards, we induced a phase transition from amorphous to crystalline anatase by pulsed UV-laser irradiation. A pulsed UV laser with a low penetration length was used to avoid the heating and damaging of the polymeric substrate. The diffusion of the heat and the temperature behaviour were simulated and discussed. We studied experimentally the effect of the laser fluence and pulse number on the amorphous-crystal transition. We observed the presence of two thresholds for the formation of the crystalline phase: on the fluence and the number of laser shots. Moreover, widening of pre-existing cracks is observed, as soon as fluence and the number of pulses increase. To improve further the quality of the deposited layer, we introduced a ZnO interlayer between TiO_2 and the PMMA substrate. The effect of this interlayer was also discussed. Lastly, wettability, as a measure of the overall quality of the layer, was measured and interpreted by using the Cassie model.

1. Introduction

TiO_2 is one of the most studied oxides since the work of Fujishima, in late '70, an enormous quantity of studies has been performed on the photocatalytic properties of this material. It is potentially able to reduce the problem of environmental pollution in water and in air which is considered one of the major humanity issues by several governative and non-governative institutions. This material is photo-active in the oxidation of contaminants, it is also stable, cheap, non-toxic, and biocompatible [1–4]. As it is well known, irradiated TiO_2 with UV light (larger than 3 eV) can induce the generation of hole with a high oxidation power [1]. These holes, reaching the liquid-solid interface, can oxidize the organic compounds present in water, up to their complete mineralization [3]. This fact paves the way for the realization of innovative devices for wastewater purification or self-cleaning, self-sterilizing surface applications [5–7].

The methodology of water treatment by using TiO_2 is however hindered by some important factors: the most important one is the low efficiency; this aspect could be overcome by reducing the size of TiO_2 materials to nanometer scale to have a high surface/volume ratio. On the other side, nanomaterials dispersed in water must be recollected at the end of the purification process, introducing a further treatment step. A method to overcome this limitation consists of the deposition of TiO_2 on low-cost substrates such as polymeric materials. In such a way, the inorganic material is firmly anchored to the substrate and the further recollection step is unnecessary [8–15].

In the literature, TiO_2 is deposited by using several methodologies Noh et al. used a sol-gel synthesis followed by a spin-coating process at 130 °C [16]. TiO_2 is deposited at room temperature without any further thermal treatment by Wu et al. [17]. An inductively coupled plasma-enhanced CVD or sputter methodology allows to deposit Anatase films at temperature from 150 °C down to 75 °C [18,19]. Further, Nb-doped Anatase TiO_2 films, grown by radio-frequency magnetron sputtering and thus irradiated by a KrF excimer laser (0.25 J/cm^2), is used as transparent electrodes in flexible organic solar cells [20].

In the present paper, we investigate the potentiality of the low-

* Corresponding author.
E-mail addresses: massimo.zimbone@ct.infn.it (M. Zimbone), maria.cantarella@ct.infn.it (M. Cantarella), federico.giuffrida@dfa.unict.it (F. Giuffrida), francesco.lavia@imm.cnr.it (F. La Via), vittorio.privitera@cnr.it (V. Privitera), enrico.napolitani@unipd.it (E. Napolitani), giuliana.impellizzeri@ct.infn.it (G. Impellizzeri).

https://doi.org/10.1016/j.mssp.2023.107328
Received 15 July 2022; Received in revised form 28 October 2022; Accepted 8 January 2023
Available online 20 January 2023

temperature atomic layer deposition technique for the realization of TiO_2 – based hybrid photocatalysts. The atomic layer deposition (ALD) allows depositing a very thin layer of TiO_2, with high precision and quality, also on nanostructured surfaces [21–24]. However, to have good quality anatase TiO_2, we need to deposit at a temperature such high as 300 °C [25,26]. At this temperature, most of the polymers are not stable and undergo melting, degradation, or decomposition. So, only a deposition temperature lower than the glass transition temperature can be used. The polymer of our choice was polymethyl methacrylate (PMMA), for its resistance to UV light, visible transparency, mechanical properties, stability, and low cost. For PMMA, the glass transition temperature is around 100 °C. Unfortunately, at this temperature, the deposition of amorphous inactive TiO_2 was usually observed [27]. A way to overcome the problem could be a further step of crystallization induced by pulsed laser treatment. Indeed, laser pulses can induce a local increase of the temperature surface, leaving the underlying substrate cold, avoiding in this way the melting/decomposition of the polymer. For all these reasons, we investigated the possibility of a laser-induced phase transition from amorphous to crystalline TiO_2 without the degradation of the polymer. The right choice of the laser parameters is very important; indeed, by selecting the appropriate wavelength and temporal pulse length, we can control both the penetration length and the heat diffusion length. Moreover, by selecting the appropriate fluence, we can control the maximum temperature reached on the TiO_2 surface and the TiO_2/PMMA interface avoiding any degradation of the polymer. For these reasons, we chose a UV pulsed KrF excimer laser working in the nanosecond range length. We, thus, investigated the effect of the laser fluence and the number of laser pulses on the morphology, crystallinity, and overall quality of the film. We paid also particular attention to the stability of the crystalline layer on the polymeric substrate.

Lastly, we used two standard methodologies (ALD deposition and laser annealing) to realise an innovative combined methodology able to obtain high-quality photoactive anatase on polymeric substrate. This methodology is industrially scalable and can also produce photo-induced wettability changing layer with high-quality on polymer. This can pave the way for a widening of the use of plastic substrates and also for the use of TiO_2.

2. Materials and methods

2.1. ALD deposition

Before the experiment, the PMMA substrates, used in this work and with a thickness of 4 mm, were washed with de-ionized water and isopropanol and then dried under nitrogen flux. Czochralski (100)-oriented silicon was also employed as a reference substrate for the ALD process.

TiO_2 films were deposited by an Atomic Layer Deposition reactor at 90 °C. We used the Picosun R-200 Advanced reactor. The employed ALD precursors were $TiCl_4$ (purity ≥99.9995%) for Ti and and de-ionized pure water for O. Carrier and purge gas was N_2 (purity ≥99.999%). The pulse and purge time were kept constant at 0.1/3/0.1/5 s for $TiCl_4$/N_2/H_2O/N_2, while different cycles were set from 100 to 6400 so to induce different TiO_2 layer thicknesses.

2.2. Laser treatment

The amorphous TiO_2 film deposited by ALD was irradiated at 248 nm by a KrF excimer laser (Coherent COMPex 201F). Pulse duration was set to 21 ns. Spot was a square of 5 × 5 mm^2 in size (2% uniformity, 1% reproducibility and 2% accuracy). The experiments were performed at 10 Hz. The energy densities were varied from 30 to 80 mJ/cm^2. The pulses were varied from 1 to 200. The energy densities can be controlled with 1% accuracy through a motorized attenuator paired with an in-line energy meter. The penetration depth of the KrF laser in TiO_2 was estimated to be ~9 nm (considering the absorption coefficient to be 1.06 × 10^6 cm^{-1}) [28].

2.3. Characterizations

A HR800 integrated system by Horiba Jobin Yvon, is used for acquiring Raman spectra. We worked in a back-scattering configuration with a coaxial optics (with a dichroic mirror for 325 nm light) and a UV grade × 40 objective. A He–Cd laser with a wavelength of 325 nm and power in the range between 1 and 10 mW was used. The penetration depth of the He–Cd laser in TiO_2 was estimated to be ~35 nm (considering an absorption coefficient of TiO_2 of 2.9 × 10^5 cm^{-1}) [28]. Spectra acquired in different points (realizing the map) were summed and a final spectrum was obtained. The spatial resolution achievable for maps was 2 μm. The power density ranges between 0.5 and 5 kW/cm^2 was reached. The Raman emitted light was dispersed by 1800 grooves/mm kinematic grating. To acquired maps the surface of each sample was scanned with a step of 10 μm. We acquired a spectrum for each point. The area of the map was 100 × 100 μm^2. Spectra acquired inside (or outside) the laser spots were averaged reducing the errors. A laser-irradiated region was individuated and the Raman map was performed near the edge of the spot. In this way, we observed in the same map both the irradiated region and the as-deposited material.

Optical microscopies were performed with an Olympus BX40 microscope. The configuration of the bright field was used.

SEM images were acquired with a Gemini field emission SUPRA 25 Carl Zeiss microscope.

The films thickness was evaluated by ellipsometric measurements. We used a Woollam M − 2000 instrument. Data were analyzed by applying a Cauchy model in the 400–1700 nm range.

The wettability of the surface was measured by using a DATAPHYSICS OCA 15 PRO contact angle measurement device. The sample surface was irradiated with UV LED light at 360 nm with an irradiance of 12 mW/cm^2 for 1 h. Contact angle (CA) was measured immediately after irradiation in order to reduce carbon contamination."

3. Results and discussion

Fig. 1a shows a schematic of the two typologies of the as-prepared samples. In the first one, a TiO_2 layer of 440 nm was deposited by ALD. The deposition temperature was set at 90 °C to avoid the degradation of the PMMA substrate. A second set of samples comprised the same TiO_2 layer with an inter-layer of 200 nm of ZnO, deposited between TiO_2 and PMMA. In Fig. 1b, as an example, a photo of the laser-treated samples is shown. Laser spots of 0.5 × 0.5 cm^2 in size are apparent as bright squares. Larger squares of 1 × 1cm^2 were also realized by combining four spots to have samples with larger areas to be analyzed. The difference in colours of different spots, from almost transparent to white, reflects the different laser irradiation conditions: both the number of pulses and fluencies were changed. The scope of the factors affecting the visual aspect of the spots could be very complex and related to the formation of a crystalline film and to the roughening of the surface. The regions between spots was not interested in the laser irradiation and are used as reference ("as-deposited").

Fig. 2 reports the Raman analyses performed on TiO_2/PMMA samples. Fig. 2a shows an example of Raman spectra of irradiated and not irradiated TiO_2 regions. For as-deposited TiO_2 a broad unstructured peak is observed at about 550 cm^{-1}, indicating the amorphous structure of the as-deposited titania films. While, in the region irradiated at 50 mJ/cm^2 with 10 pulses, the spectrum presents the peculiar features of the crystalline TiO_2 in the anatase phase. The main peaks are located at 153, 399, 520, and 637 cm^{-1} and they are assigned to E_g, B_{1g}, A_{1g} ed E_g peaks of anatase, respectively [29,30]. For all samples displaying crystalline phase, the line position and linewidth of these peaks remains constant (inside the experimental errors) while the intensity of the peaks at 399, 520, and 637 cm^{-1} (B_{1g}, A_{1g} ed E_g) results proportional to the intensity of 153 cm^{-1} peak (E_g) that is the most prominent peak. Thus, it

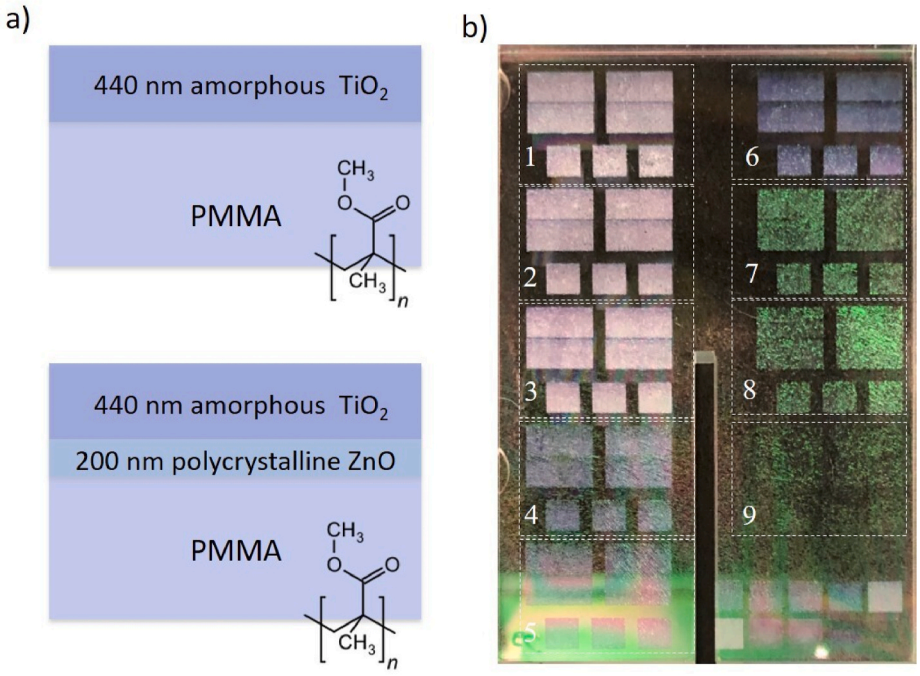

Fig. 1. a) Scheme of the "as deposited" samples in cross section before laser irradiation; b) Photo of a sample taken as example. Laser spots are apparent as bright squared regions of 0.5x0,.5 cm^2 (or 1 × 1 cm^2) in size. Different brightness and colours are due to different irradiation conditions in particular the numbered rectangle represent spots in which the same condition are used. Fluence (in mJ/cm^2) and number of pulses are reported here for each highlighted square: 1) 60,200 2) 60,100 3) 60,10 4) 50,200 5) 50,100 6) 50,10 7) 40,200 8) 40,100 9) 40,10.

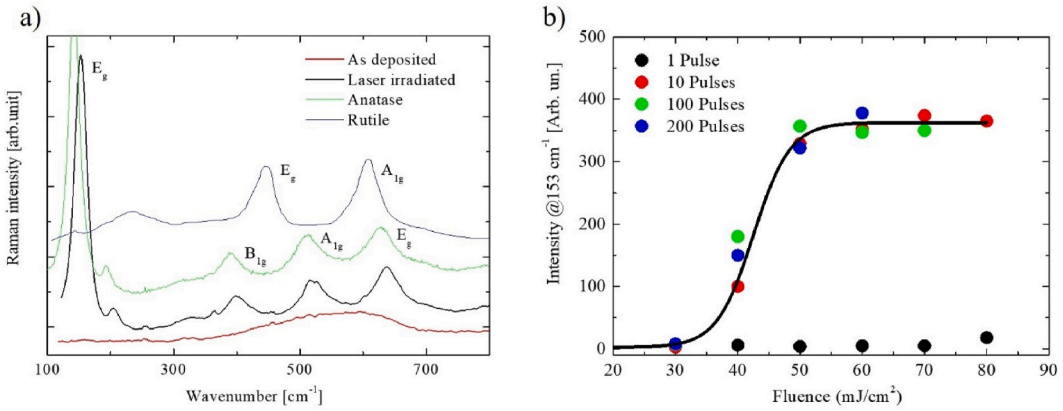

Fig. 2. a) Example of Raman spectra of "as deposited" and laser irradiated samples. E_g, B_{1g} A_{1g} E_g peaks at 153, 399, 520, 637 cm^{-1} respectivelly are shown after laser irradiation. Rutile and Anatase peaks are also shown for comparison puroses. b) Intensity of the E_g peak at 153 cm^{-1} as a function of laser fluence for different laser pulses. Black curve is a guide for the eyes.

is used in the present paper as a signature for the presence of the crystalline phase. In Fig. 2b is shown this intensity (at 153 cm^{-1}) as a function of laser fluence for different laser pulses on TiO_2/PMMA. It is apparent that for 1 pulse, the intensity of the peak remains negligible indicating that the film is amorphous whatever the fluence (in the explored range: 30–80 mJ/cm^2). For 10 pulses, and fluence lower than 40 mJ/cm^2 (i.e. 30-40 mJ/cm^2), the signal remains negligible; while, when the fluence raises at 50 mJ/cm^2, we observed an abrupt increase of the intensity indicating that the crystallization occurs. At fluences higher than 50 mJ/cm^2, the peak's intensity reaches a saturation level. The high intensity of the peaks is a clear feature of the crystallization phase in the thickness probed by the Raman measurements (i.e., 60 nm). A threshold for the TiO_2 crystallization between 40 and 50 mJ/cm^2 can be advised; in particular, fitting with a suitable sigmoid function, it is possible to evaluate a threshold of 43 ± 2 mJ/cm^2. The same trend and the same maximum intensity value are found for the samples irradiated with a higher number of pulses (100 and 200 pulses). Moreover, no phase transition to TiO_2 rutile is observed in the explored range of fluence even for the high number of pulses.

Considering the Raman results, the formation of a crystalline TiO_2 layer on the surface of the sample is expected. We performed ellipsometric analyses to measure the thickness of the crystallized layers. We assume that the sample is constituted by two layers of amorphous and crystalline Anatase TiO_2 respectively. In Fig. 3, we report the thickness of the amorphous and crystallized layer as a function of the fluence for different number of pulses. As the fluence increases, the thickness of the crystallized layer increases (and the thickness of the amorphous layer decreases accordingly). The solid line represents the simulated thickness: it will be discussed in the next paragraph. The thickness of the crystallized layer after 1 pulse (not shown) is negligible. We want to highlight that the thickness of the layer depends on the fluence and has a negligible dependence on the number of pulses. Moreover, the sum of the thickness of the amorphous and crystallized layer is almost constant corroborating the fact that the total film thickness remains almost constant.

In order to understand the process, the evolution of the temperature

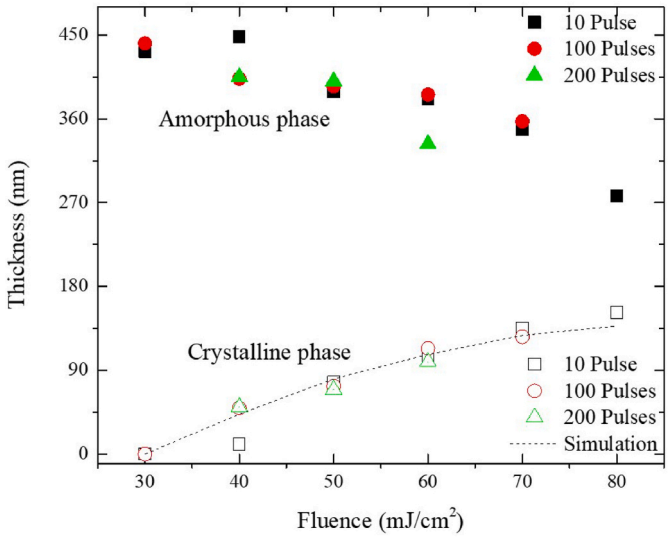

Fig. 3. Ellipsometric thickness of the amorphous and crystalline TiO_2 layer as a function of fluence for different number of pulses. The dotted line represent the thickness in which the temperature, in the simulation, is higher than the amorphous-crystal transition temperature.

in the laser-irradiated samples was evaluated by simulation. We solved the unidimensional heat diffusion equation:

$$\rho C_p \frac{\partial T}{\partial t} = \alpha I(z,t) + k\frac{\partial^2 T}{\partial z^2} \quad (1)$$

$$I_{(z,t)} = I_0(t)(1-R)e^{-\alpha z} \quad (2)$$

where T represents the absolute temperature, ρ is the sample density, C_p is the specific heat, k is the thermal conductivity, I_0 is the laser intensity at the surface, R is the surface reflectivity, α is the optical absorption, z is the depth from surface, and $I(z,t)$ is the laser intensity [31]. Simulations of the temperature depth profiles as a function of the time during the laser processes were performed through numerical solutions of the heat equation (LIMP - the Harvard simulation software package) [31], based on heat flow calculations calibrated on TiO_2, ZnO, and PEN physical and optical literature data [32–38]. In Fig. 4, the temperature temporal evolution at the surface and at the interface with the polymer for the TiO_2/PMMA samples is reported. Fluencies ranged from 30 (under the crystallization threshold) to 60 mJ/cm^2 (above the crystallization

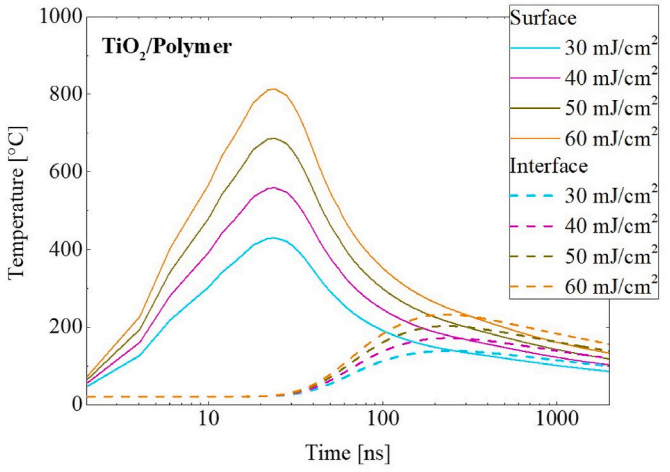

Fig. 4. Simulation of the temperature as a function of time in two different location of the sample: at surface (full line) and interface between TiO_2/polymer (dotted line).

threshold). The increase of the temperature due to the laser heating is apparent, and a peak at 25 ns is observable. At the surface, for 60 mJ/cm^2, the highest estimated temperature is about 800 °C. This temperature is above the amorphous-anatase temperature (over 400 °C) in a pure TiO_2 under thermal equilibrium [39]. Nevertheless, it is worth noting that temperatures higher than 400 °C are reached for less than 100 ns. Moreover, the simulation allows to evaluate the thickness of the TiO_2 in which the temperature overcome the amorphous-crystal transition temperature. This thickness is reported in Fig. 3 as a dotted line. As it is apparent from the figure, the calculated curve is in accordance with the thickness of the crystallized layer measured ellipsometricaly. This agreement corroborates the use of the simulation results with respect to the experimental ones. Another important feature is the maximum temperature and the asymptotic temperature (evaluated 2 μs after the pulse) at the interface between the titanium dioxide and the polymer. Let's again consider the curve obtained for 60 mJ/cm^2, the maximum interface temperature was about 200 °C after 300 ns and decrease to 150 °C, after 2 μs.

3.1. *Effect of the interlayer*

The same experimental analyses and simulations, were also performed on TiO_2/ZnO/PMMA samples. In particular Raman intensity of the peak at 153 cm^{-1} for the samples with the ZnO interlayer follows the same trend and it has the same threshold fluence and saturation value of the above-described sample without the interlayer (i.e., TiO_2/PMMA). The variation in the intensity of the peak at 153 cm^{-1} for the TiO_2/ZnO/PMMA samples is reported in Fig. 1S.I. Even in this set of samples, at least 10 pulses and more than 40 mJ/cm^2 in fluence are necessary to induce the crystallization of the deposited TiO_2 layers. Ellipsometric analyses show the same results obtained for the samples without interlayer. Also the simulations resulted very similar to those obtained for the samples without the interlayer. The same trend of TiO_2/PMMA samples is found for the TiO_2/ZnO/PMMA samples. It is reported in Fig. 2 S.I. The negligible difference in the temperature behavior at the surface can be observed in the first 100 ns indeed in this temporal range, the diffusion process is negligibly influenced by the ZnO interlayer. On the other side, the temperature at the interface with PMMA is reduced from 200 °C to about 120 °C thanks to the ZnO interlayer.

Although the Raman and ellipsometric measurements did not reveal any substantial differences for the two sets of samples (TiO_2/PMMA and TiO_2/ZnO/PMMA), the surface morphology is heavily influenced by the laser treatment. Fig. 5 shows the optical microscopies of the samples irradiated at 60 mJ/cm^2 with different pulses (1, 10, or 100 pulses). The TiO_2/PMMA sample irradiated with 1 pulse has a surface similar to the as-deposited film. The cracks widen with the number and fluence of the pulses. At 10 pulses large clod of about a hundred microns in size are apparent. The separation between clods is larger than that found in the "1 pulse" sample. For 100 pulses, the dimension of the cracks increases further leading to isolated small clods. The quality of the layer improves after the introduction of the ZnO interlayer (TiO_2/ZnO/PMMA). The as-deposited and 1 pulse irradiated samples present a smooth surface with no cracks. Sample irradiated with 10 pulses shows very large smooth zones (in the mm scale length) due to the very limited presence of cracks. This is in contrast with the TiO_2/PMMA sample where the surface is more fractured. The TiO_2/ZnO/PMMA sample irradiated with 100 pulses is poor in quality and is similar to the TiO_2/PMMA sample irradiated with 100 pulses. The laser fluence had a large impact on the structure of the films; in Fig. 2 S.I. and 3 S.I. we reported the optical microscopies of the irradiated samples for different fluencies (50, 60, 70, or 80 mJ/cm^2) and pulses number (1, 10, or 100 pulses). In particular, Fig. 2 S.I. reports the microscopies of the TiO_2/PMMA samples, while Fig. 3 S.I. reports the microscopies of TiO_2/ZnO/PMMA samples. For 1 and 100 (or more) pulses only a slight dependence of the laser fluence can be noted. On the contrary for the 10 pulses (second row of Fig. 2 S.I. and 3 S.I.), the samples "with" and "without" the interlayer are very

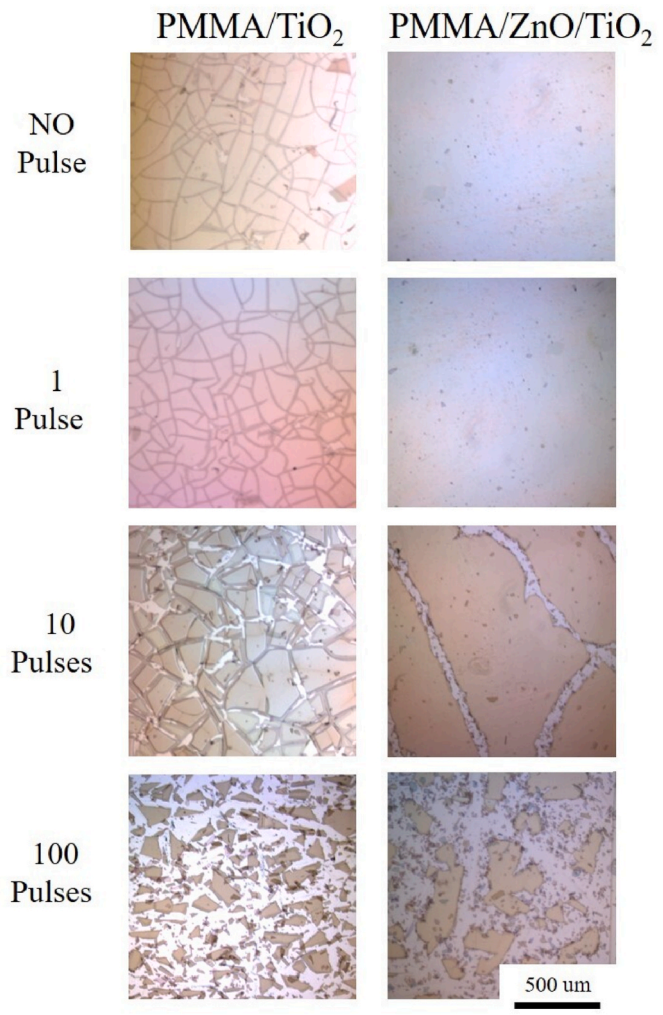

Fig. 5. Optical microscopies of laser irradiated TiO_2/PMMA (left column) and TiO_2/ZnO/PMMA (right column) samples irradiated at 60 mJ/cm^2. Number of pulses are indicated on the left side of the figure. Scale bar is the same for all images.

different. Nevertheless, increasing the fluence from 50 to 70 mJ/cm^2 the size of the cracks increases reducing the size of the clods. This effect is apparent in both cases.

Crystalline TiO_2 is well known to transit to the photo-induced hydrophilic state after UV irradiation. A large number of applications of TiO_2 depend on this valuable property so it is important to evaluate if synthesized samples display wettability change after irradiation. This is even more important with the presence of ZnO layer, because due to the energy band alignment of ZnO and TiO_2, both electrons and holes, generated from light excitation, could be transferred from TiO_2 to ZnO reducing the TiO_2 activity. This could reduce or completely cancel the photocatalytic activity. The wettability measurements were reported only for TiO_2/ZnO/PMMA samples because of their smooth starting surface (with few cracks). In Fig. 6, the contact angle is reported as a function of the fluence for samples irradiated with a different number of pulses. For the as-deposited surface (black line in Fig. 6) and laser-irradiated with 1 pulse, the contact angle remained almost constant at about 80° showing low hydrophilicity of the surfaces. For 10 pulses and fluence lower than 50 mJ/cm^2 (i.e., 30 and 40 mJ/cm^2) the contact angle remained ~80°, while at 50 mJ/cm^2 we observed an abrupt decrease of the contact angle approaching 20°, indicating good hydrophilicity of the investigated surfaces. This is in agreement with the Raman results where the crystallization of the deposited layer appeared at ~43 mJ/cm^2. Nevertheless, at higher fluences (70 and 80 mJ/cm^2),

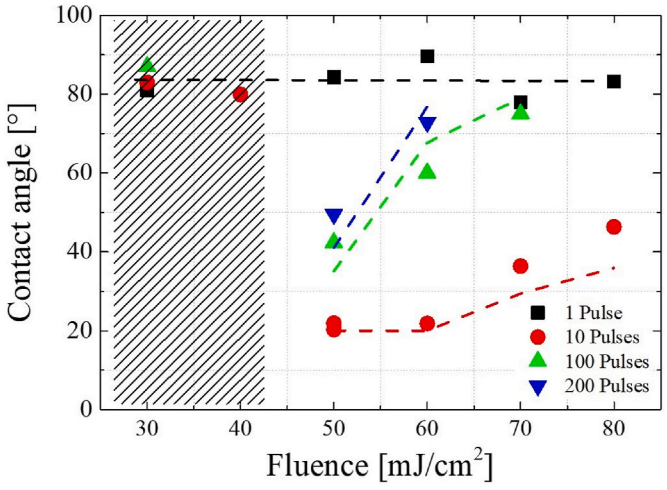

Fig. 6. Contact angle of laser irradiated TiO_2/ZnO/PMMA samples as a function of fluence for different number of pulses. Lines are calculated by Cassie model as explained in the text.

the contact angle increases approaching ~ 50°. For 100 and 200 pulses even at 40 mJ/cm^2, the contact angle resulted in ~50° and it increases with the fluence, indicating a deterioration of the film surfaces.

3.2. Discussion

Raman and ellipsometric analysis (see Figs. 2 and 3), showed that for 1 pulse, the intensity of the peak at 153 cm^{-1} is negligible irrespective of the used laser fluence. This indicates that the single shot irradiation was unable to induce a phase transition from amorphous to anatase. On the contrary, the simulations showed that the temperature raised to approximately 800 °C during the laser pulses for 60 mJ/cm^2 in fluence. This value should be enough to have the transition from amorphous to anatase and from anatase to rutile phase. Nevertheless, the temperature remained higher than 400 °C for a very short period (100 ns). Considering that the process of crystallization from amorphous to anatase has a slower kinetic than 100 ns [26] and taking into account the latent heat, the crystallization was kinetically hindered for such a fast process such as 1 laser pulses. For 10 or more pulses, the behaviour depends on the fluence. For fluencies below the threshold of 43 mJ/cm^2, the increase of the temperature was not sufficient to induce a phase transition: Raman, optical microscopy, and contact angle remained the same to the as-deposited sample whatever the number of the pulses. On the contrary, above the threshold fluence, the temperature higher (than the amorphous-crystalline temperature) allows the transition to anatase and further the high number of pulses is enough to allows kinetics to evolve. Note that for 10 pulses, the total time in which the surface remains at temperature above the amorphous/anatase phase transition temperature can be estimated to be of the order of 1 μs. It should be enough to kinetically allow the transition. Once the crystalline phase is formed, the Raman signal at 153 cm^{-1} resulted in a high value (Fig. 2b) and changes in surface morphology (Fig. 5) and in contact angle (Fig. 6) occurred. Regarding the morphology, we could speculate that cracks enlargement is attributed to the induced thermal stress on the edge of TiO_2 clods, or to an increase of the density of the crystalline layer with respect to the amorphous phase that shrinks the crystalline layer (density of amorphous, and anatase phases are 3.2, and 3.8 g/cm^3 respectively) [39]. For 100 (or more) pulses, the films appeared discontinuous and with very low quality (see Figs. 5 and 100 pulses) due to the large size of the cracks even at fluence just above the threshold fluence (50 mJ/cm^2).

Let's now consider the case of the samples with the ZnO interlayer. Simulations showed that the temporal evolution of the heat transfer in the samples with and without the ZnO interlayer suffers of only small

differences (see Figs. 4 and 2 S.I.). The spatial distribution of the temperature after 25 ns, (i.e. at peak of the laser pulse) indicated that only a small fraction of the layer (~100 nm), is influenced by the high temperature (>500 °C). This consideration explains why crystallization threshold and heat behaviour are very similar for both samples (with and without the interlayer).

Nevertheless, the morphology of the two kind of films appeared different: the samples without the ZnO interlayer (TiO_2/PMMA) were more cracked if compared to the samples with the interlayer (TiO_2/ZnO/PMMA), as shown in Fig. 5. The cracks in the TiO_2/PMMA samples were present even in the as-deposited samples and their size enlarges with the laser irradiation. Cracks in the TiO_2/ZnO/PMMA samples were almost missing in the as-deposited samples, and the cracks density remains very low in the irradiated samples. We noted that, due to irradiation, cracks widen reducing the size of the clods (see Fig. 3 S.I.), and consequently the quality of the layer decreases. So the quality of the film seems correlated to the presence of pre-existing cracks (present in the sample, before the laser treatment). These cracks should, in turn, depend on the deposition methodology. The atomic layer deposition of inorganic metal oxides films on polymers is a demanding process due to the lack of reactive surface sites on polymers [40]. Nevertheless, nucleation of the metal-oxide is possible by the diffusion and entrapment of the ALD precursors into the polymers [41]. As the deposition proceeds, the nucleation sites coalesce and form metal oxide film on top of the polymeric substrate. In our case, we can speculate that the nucleation site density of TiO_2 and ZnO are different with the used experimental condition and with the peculiar polymer used. This could bring to the larger clods in the film with the ZnO interlayer and to a difference in the final morphology. This consideration is supported by the optical microscopies in Figs. 5 and 3 S.I.,4 S.I. and SEM analyses reported in Fig. 5 S.I where it is apparent that the TiO_2/PMMA surface results covered by smaller clods (and thus it is more cracked) than the TiO_2/ZnO/PMMA sample counterpart. Considering the obtained results, we can conclude that the presence of the ZnO interlayer is important for the anchoring of the TiO_2 layer on PMMA, in reducing the presence of cracks that act as a "critical" zone under laser irradiation.

When crystalline TiO_2, with good photo-catalytical activity, is irradiated with UV radiation, it eliminates the contaminants on the surface and structural changes on its surface occurs (generation of light-induced vacancies and Ti^{3+} states) [42,43]. These effects induce an increase of the surface affinity with hydroxyl groups (by dissociation of chemisorbed water molecule) and the formation of hydrophilic domains. On the contrary, for amorphous or "not active" TiO_2, wettability remains unchanged upon UV irradiation. In our case, the contact angle was around 80° for both amorphous, and non-irradiated samples. Low values (~20°) were obtained only for crystallized (Fig. 2b) and not cracked films (Fig. 3) i.e. for fluencies between 50 and 60 mJ/cm^2 and 10 pulses. The presence of cracks at higher fluence and/or at higher number of pulses, makes more complex the surface morphology and thus the interpretation of the data. Indeed, the contact angle is highly dependent on the texture of the surface. In our case, we found that increasing the fluence, cracks and zones without film appears. We can schematize the surface as composed (after UV illumination) with regions with hydrophilic character (TiO_2) and regions with less hydrophilic character (polymer). For heterogeneous surfaces wettability properties are described by Cassie model [43]. According to this model the apparent contact angle for a liquid droplet is related to the contact angle of the "bare" TiO_2 and "bare" polymer by the equation:

$$\cos(\theta_{app}) = f\cos(\theta_{Tio2}) + (1-f)\cos(\theta_{polymer}) \quad (3)$$

where f is the area fraction of the liquid droplet in contact with the TiO_2 surface, (1-f) area fraction in contact with the polymer and θ_{TiO2}, $\theta_{polymer}$, θ_{app}, are the contact angle of TiO_2, the polymer and the apparent (measured) one. The values of the area fraction can be smoothly measured by the optical images in Figs. 5 and 3 SI and 4 SI while the contact angle of the "bare" TiO_2 and that of the polymer are assumed to be 20° and 80° respectively. In such a way, we are able to calculate the apparent contact angle and compare it with the measured one. Results are shown in Fig. 6 as dotted lines. Although the simple model used, the results shows the same trend of the experimental observation. This corroborated that the model used can describe quite well the properties of the surface. Indeed, as the surface becomes crystalline the contact angle goes down to 20° making the surface hydrophilic but increasing the fluence the presence of cracks and the peeling off of the TiO_2 exposes the "less hydrophilic" polymer surface to the water environment, making the contact angle higher.

4. Conclusions

We deposited through low temperature (90 °C) ALD technique a thin layer of 400 nm of amorphous TiO_2 on PMMA. Pulsed UV-laser irradiation induced a phase transition from amorphous to crystalline anatase phase. To have the crystallization and good quality of the layer, some requisites should be matched: fluences and pulses number have to overcome a threshold value of ~45 mJ/cm^2 and 10 pulses, respectively. Simulations of the heat diffusion demonstrated that the temperature on the surface overcame the phase transition temperature, but to have a crystallized layer at least 10 pulses are necessary. Moreover, we found that the quality of the anatase layer was limited by the presence of cracks: at higher fluences (or pulses number) the size of the cracks increases. Nevertheless, improvement of the layer quality was obtained by introducing a ZnO interlayer between TiO_2 and the PMMA polymer. Wettability properties of the surface are described by using the Cassie model.

CRediT authorship contribution statement

Massimo Zimbone: Writing – original draft, Investigation, Formal analysis, Conceptualization. **Maria Cantarella:** Writing – review & editing, Visualization. **Federico Giuffrida:** Investigation. **Francesco La Via:** Supervision. **Vittorio Privitera:** Supervision. **Enrico Napolitani:** Investigation, Conceptualization. **Giuliana Impellizzeri:** Validation, Supervision, Conceptualization.

Declaration of competing interest

The authors declare that they have no known competing financial interests or personal relationships that could have appeared to influence the work reported in this paper.

Data availability

No data was used for the research described in the article.

Acknowledgments

The authors wish to thank Giuseppe Pantè (CNR-IMM), Luca Bacci (University of Padova) and Nicola Argiolas (University of Padova) for their technical assistance. This work has been funded by the national project PON TARANTO (CUP: B86C18000870005), and by the University of Padova (grant UNIPD-ISR 2017 "SENSITISE").

Appendix A. Supplementary data

Supplementary data to this article can be found online at https://doi.org/10.1016/j.mssp.2023.107328.

References

[1] A. Fujishima, X. Zhang, D.A. Tryk, TiO_2 photocatalysis and related surface phenomena, Surf. Sci. Rep. 63 (2008) 515–582.

[2] Akira Fujishima, Kenichi Honda, Electrochemical photolysis of water at a semiconductor electrode, Nature 238 (5358) (1972) 37–38, https://doi.org/10.1038/238037a0.

[3] A. Fujishima, T.N. Rao, D.A. Tryk, Titanium dioxide photocatalysis, J. Photochem. Photobiol. C Photochem. Rev. 1 (1) (2000) 1–21, https://doi.org/10.1016/S1389-5567(00)00002-2.

[4] X. Chen, S.S. Mao, Titanium dioxide nanomaterials: synthesis, properties, modifications, and applications, Chem. Rev. 107 (2007) 2891–2959, https://doi.org/10.1021/cr0500535.

[5] Z. Zhao, J. Tian, Y. Sang, A. Cabot, H. Liu, Structure, synthesis, and applications of TiO2 nanobelts, Adv. Mater. 27 (16) (2015) 2557–2582, https://doi.org/10.1002/adma.201405589.

[6] R. Katal, S. Masudy-Panah, M. Tanhaei, M.H.D.A. Farahani, H. Jiangyong, A review on the synthesis of the various type of anatase TiO2 facets and their applications in photocatalysis, Chem. Eng. J. 384 (123384) (2020) 1–26, https://doi.org/10.1016/j.cej.2019.123384.

[7] W. Zhang, Y. Tian, H. He, L. Xu, W. Li, D. Zhao, Recent advances in the synthesis of hierarchically mesoporous TiO2 materials for energy and environmental applications, Natl. Sci. Rev. 7 (2020) 1702–1725, https://doi.org/10.1093/nsr/nwaa021.

[8] G. Impellizzeri, V. Scuderi, L. Romano, P.M. Sberna, E. Arcadipane, R. Sanz, M. Scuderi, G. Nicotra, M. Bayle, R. Carles, F. Simone, V. Privitera, Fe ion-implanted TiO2 thin film for efficient visible-light photocatalysis, J. Appl. Phys. 116 (173507) (2014) 1–8, https://doi.org/10.1063/1.4901208.

[9] G. Impellizzeri, V. Scuderi, L. Romano, E. Napolitani, R. Sanz, R. Carles, V. Privitera, C ion-implanted TiO2 thin film for photocatalytic applications, J. Appl. Phys. 117 (105308) (2015) 1–6, https://doi.org/10.1063/1.4915111.

[10] V. Scuderi, G. Impellizzeri, M. Zimbone, R. Sanz, A. Di Mauro, M.A. Buccheri, M. Miritello, A. Terrasi, G. Rappazzo, G. Nicotra, V. Privitera, Rapid synthesis of photoactive hydrogenated TiO2 nanoplumes, Appl. Catal., B 183 (2016) 328–334, https://doi.org/10.1016/j.apcatb.2015.10.055.

[11] V. Scuderi, M.A. Buccheri, G. Impellizzeri, A. Di Mauro, G. Rappazzo, K. Bergum, B. Svensson, V. Privitera, Photocatalytic and antibacterial properties of titanium dioxide flat film, Mater. Sci. Semicond. Process. 42 (2016) 32–35, https://doi.org/10.1016/j.mssp.2015.09.005.

[12] V. Scuderi, G. Impellizzeri, L. Romano, M. Scuderi, M.V. Brundo, K. Bergum, M. Zimbone, R. Sanz, M.A. Buccheri, F. Simone, G. Nicotra, B.G. Svensson, M. G. Grimaldi, V. Privitera, An enhanced photocatalytic response of nanometric TiO_2 wrapping of Au nanoparticles for eco-friendly water applications, Nanoscale 6 (2014) 11189–11195, https://doi.org/10.1039/c4nr02820a.

[13] M. Zimbone, M.A. Buccheri, G. Cacciato, R. Sanz, G. Rappazzo, S. Boninelli, R. Reitano, L. Romano, V. Privitera, M.G. Grimaldi, Photocatalytical and antibacterial activity of TiO_2 nanoparticles obtained by laser ablation in water, Appl. Catal., B 165 (2015) 487–494, https://doi.org/10.1016/j.apcatb.2014.10.031.

[14] G. Sanzone, M. Zimbone, G. Cacciato, F. Ruffino, R. Carles, V. Privitera, M. G. Grimaldi, Ag/TiO_2 nanocomposite for visible light-driven photocatalysis, Superlattice. Microst. 123 (2018) 394–402.

[15] M. Zimbone, G. Cacciato, M.A. Buccheri, R. Sanz, N. Piluso, R. Reitano, F. La Via, M.G. Grimaldi, V. Privitera, Photocatalytical activity of amorphous hydrogenated TiO_2 obtained by pulsed laser ablation in liquid, Mater. Sci. Semicond. Process. 42 (2016) 28–31.

[16] H. Noh, S.G. Oh, S.S. Im, Preparation of anatase TiO_2 thin film by low temperature annealing as an electron transport layer in inverted polymer solar cells, Appl. Surf. Sci. 333 (2015) 157–162, https://doi.org/10.1016/j.apsusc.2015.02.010.

[17] C.H. Wu, H. Li, H.H. Fong, V.A. Pozdin, L.A. Estroff, G.G. Malliaras, Room-temperature preparation of crystalline TiO_2 thin films and their applications in polymer/TiO_2 hybrid optoelectronic devices, Org. Electron. 12 (2011) 1073–1079, https://doi.org/10.1016/j.orgel.2011.03.004.

[18] D. Li, N. Gautier, B. Dey, S. Bulou, M. Richard-Plouet, W. Ravisy, A. Goullet, P. Choquet, A. Granier, TEM analysis of photocatalytic TiO_2 thin films deposited on polymer substrates by low-temperature ICP-PECVD, Appl. Surf. Sci. 491 (2019) 116–122.

[19] G.D. Rajmohan, F.Z. Huang, R. D'Agostino, J. Du Plessis, X.J. Dai, Low temperature reactively sputtered crystalline TiO_2 thin film as effective blocking layer for perovskite solar cells, Thin Solid Films 636 (2017) 307–313.

[20] J.H. Lee, C.C. Lin, Y.C. Lin, Transparent conducting Nb-doped TiO_2 electrodes activated by laser annealing for inexpensive flexible organic solar cells, Jpn. J. Appl. Phys. 51 (2012) 1–4, https://doi.org/10.1143/JJAP.51.015502.

[21] N. Pinna, M. Knez, Atomic Layer Deposition of Nanostructured Materials, Wiley-VCH, Weinheim, Germany, 2012.

[22] J.D. Ferguson, A.W. Weimer, S.M. George, Atomic layer deposition of Al2O3 films on polyethylene particles, Chem. Mater. 16 (2004) 5602–5609, https://doi.org/10.1021/cm040008y.

[23] C.A. Wilson, R.K. Grubbs, S.M. George, Nucleation and growth during Al2O3 atomic layer deposition on polymers, Chem. Mater. 17 (2005) 5625–5634, https://doi.org/10.1021/cm050704d.

[24] X. Liang, S.M. George, A.W. Weimer, N.-H. Li, J.H. Blackson, J.D. Harris, P. Li, Synthesis of a novel porous polymer/ceramic composite material by low-temperature atomic layer deposition, Chem. Mater. 19 (2007) 5388–5394, https://doi.org/10.1021/cm071431k.

[25] X. Liang, S.M. George, A.W. Weimer, N.-H. Li, J.H. Blackson, J.D. Harris, P. Li, Synthesis of a novel porous polymer/ceramic composite material by low-temperature atomic layer deposition, Chem. Mater. 19 (2007) 5388–5394.

[26] H. Zhang, J.F. Banfield, Structural characteristics and mechanical and thermodynamical properties of nanocrystalline TiO2, Chem. Rev. 114 (2014) 9613–9644.

[27] S.M. George, Atomic layer deposition: an overview, Chem. Rev. 110 (2010) 111–131, https://doi.org/10.1021/cr900056b.

[28] S. Tanemura, L. Miao, P. Jin, K. Kaneko, A. Terai, N. Nabatova-Gabain, Optical properties of polycrystalline and epitaxial anatase and rutile TiO2 thin films by rf magnetron sputtering, Appl. Surf. Sci. 212–213 (2003) 654–660, https://doi.org/10.1016/S0169-4332(03)00015-1.

[29] M. Zimbone, G. Cacciato, L. Spitaleri, R.G. Egdell, M.G. Grimaldi, A.Gulino Sb-doped titanium oxide: a rationale for its photocatalytic activity for environmental remediation, ACS Omega 3 (2018) 11270–11277.

[30] Toshiaki Ohsaka, Fujio Izumi, Yoshinori Fujiki, Raman spectrum of anatase, TiO2, J. Raman Spectrosc. 7 (6) (1978) 321–324.

[31] D.E. Hoglund, M.O. Thompson, M.J. Aziz, Experimental test of morphological stability theory for a planar interface during rapid solidification, Phys. Rev. B 58 (1998) 189–199, https://doi.org/10.1103/PhysRevB.58.189.

[32] D.G. Cahill, T.H. Allen, Thermal conductivity of sputtered and evaporated SiO2 and TiO2 optical coatings, Appl. Phys. Lett. 65 (1994) 309–311, https://doi.org/10.1063/1.112355.

[33] S.J. Smith, R. Stevens, S. Liu, A. Navrotsky, J. Boerio-Goates, B.F. Woodfield, Heat capacities and thermodynamic functions of TiO2 anatase and rutile: analysis of phase stability, Am. Mineral. 94 (2009) 236–243, https://doi.org/10.2138/am.2009.3050.

[34] Von I. Barin, Thermochemical Data of Pure Substances, VCH, Weinheim, 1989.

[35] T. Olorunyolemi, A. Birnboim, Y. Carmel, O.C. Wilson Jr., I.K. Lloyd, S. Smith, R. Campbell, Thermal conductivity of zinc oxide: from green to sintered state, J. Am. Ceram. Soc. 85 (2002) 1249–1253, https://doi.org/10.1111/j.1151-2916.2002.tb00253.x.

[36] L. Miao, S. Tanemura, M. Tanemura, S.P. Lau, B.K. Tay, Thickness-dependent optical properties of ZnO thin films, J. Mater. Sci. Mater. Electron. 18 (2007) 343–346, https://doi.org/10.1007/s10854-007-9243-3.

[37] U. Gaur, S.F. Lau, B.B. Wunderlich, B. Wunderlich, Heat capacity and other thermodynamic properties of linear macromolecules. VIII. Polyesters and Polyamides, J. Phys. Chem. Ref. Data 12 (1983) 65, https://doi.org/10.1063/1.555678.

[38] V. Vishwakarma, C. Waghela, A. Jain, Measurement of out-of-plane thermal conductivity of substrates for flexible electronics and displays, Microelectron. Eng. 142 (2015) 36–39, https://doi.org/10.1016/j.mee.2015.06.008.

[39] G.S. Chen, C.C. Lee, H. Niu, W. Huang, R. Jann, T. Schuttle, Sputter deposition of titanium monoxide and dioxide thin films with controlled properties using optical emission spectroscopy, Thin Solid Films 516 (2008) 8473–8478.

[40] N. Pinna, M. Knez, Atomic Layer Deposition of Nanostructured Materials, Wiley-VCH, Weinheim, Germany, 2012.

[41] J.D. Ferguson, A.W. Weimer, S.M. George, Atomic layer deposition of Al2O3 films on polyethylene particles, Chem. Mater. 16 (2004) 5602–5609, https://doi.org/10.1021/cm040008y.

[42] S. Banerjee, D.D. Dionysiou, S.C. Pillai, Self cleaning application of TiO2 by photo-induced hydrophilicity and photocatalysis, Appl. Catal. B Environ. 176 (2015) 396–428.

[43] A.B.D. Cassie, Contact angles, Discuss. Faraday Soc. 3 (1948) 11, https://doi.org/10.1039/DF9480300011.